SIAM J. APPL. MATH.
Vol. 80, No. 3, pp. 1290–1306

HIERARCHICAL MIXED-EFFECTS MODEL FOR HIV DYNAMICS*

YUNJEONG LEE†, YOON-GU HWANG†, HEE-DAE KWON‡, JUN YONG CHOI§, AND JEEHYUN LEE¶

Abstract. A hierarchical mixed-effects model is proposed to account for both individual- and population-level variability in human immunodeficiency virus (HIV) dynamics. This model is implemented by formulating the crucial parameters as random variables in an in-host HIV model. Model reduction is used to guide the choice for a minimal set of parameters, whose distributions are estimated by the global two-stage method. We analyze the system of ordinary differential equations with random coefficients and provide numerical simulations illustrating its asymptotic behaviors.

Key words. HIV dynamics, mixed-effects model, random ODEs

AMS subject classifications. 65, 92, 34

DOI. 10.1137/19M1246031

1. Introduction.

There have been many mathematical models that attempt to describe the interaction of CD4+ T-cells and the human immunodeficiency virus (HIV) in the immune system [8, 9, 13, 19, 21]. Mathematical models can be useful in helping to understand and predict the pathogenesis of HIV infection or to suggest a strategy that can improve patient adherence. The studies by Perelson and Nelson [19] demonstrate how mathematical models have revealed some important features of HIV pathogenesis and impacted the way in which HIV patients are treated with efficient antiretroviral drugs. Callaway and Perelson [9] investigated the ability of several biologically motivated models of HIV infection dynamics to explain sustained low viral loads. In [8], the authors suggested the dynamics of the immune response with a Michaelis–Menten-type saturation nonlinearity. Incorporation of the immune response allowed the model to exhibit transfer between unhealthy and healthy steady states through structured treatment interruptions [2].

For our study, we adopt a simple in-host model as a reasonable approximation of the dynamics for any specific individual. However, the dynamics for different individuals may vary because of the individual variability in viral production, immune response, and so on. In fact, the experimental data clearly exhibit a significant variability among patients and their responses to therapy. Hellerstein et al. [12] reported direct measurements of circulating T-cell kinetics in normal and HIV-1-infected humans where production rates of CD4+ T-cells and CD8+ T-cells vary across patients. In [11], the authors estimated the numbers of infected CD4+ T-cells and the virus they

*Received by the editors February 20, 2019; accepted for publication (in revised form) March 26, 2020; published electronically May 20, 2020.
https://doi.org/10.1137/19M1246031
Funding: The work of the third author was supported by the NRF through grant 2016R1D1A1B04931897 and by the National Research Council of Science & Technology (NST) grant by the Korea government (MSIP) through award CRC-16-01-KRICT. The work of the fifth author was supported by the NRF through grant 2015R1A5A1009350 and NRF-2016R1A2B4014178.

†Department of Computational Science and Engineering, Yonsei University, Korea (yunjung0104@gmail.com, yoongu.hwang@gmail.com).
‡Department of Mathematics, Inha University, Korea (hdkwon@inha.ac.kr).
§Department of Internal Medicine, Severance Hospital, Yonsei University College of Medicine, Korea (seran@yonsei.ac.kr).
¶Department of Mathematics & Department of CSE, Yonsei University, Korea (ezhyun@yonsei.ac.kr).

could produce by quantitative technique, which showed a wide range of values. As investigated in [2], the change in infectivity rates can move the stable equilibrium point from one associated with a high viral load to another with low viral load. Hence, the different dynamics across subjects may be attributed to differences of several crucial parameters. In this context, we employ hierarchical nonlinear mixed-effects (NLME) models to account for variations at both the individual and population levels [10].

We provide a brief overview of some hierarchical NLME models in HIV pathogenesis studies and refer the reader to a comprehensive review paper [23] on statistical methods in HIV modeling. Putter et al. considered a system of nonlinear differential equations and used short-term viral-load data to estimate the distributions of parameters [20]. The studies by Wu and Ding [24] allow variability in drug resistance and adherence in the presence of antiretroviral treatment. In [5], the authors considered a model including the immune response effector and proposed a modified algorithm to deal with the censored data. Our goal is to develop a methodology that can be used to predict the dynamics of a new patient and to suggest efficient treatment strategies for the individual patient. With this in mind, we build a hierarchical mixed-effects model by estimating the distribution of parameters across the population with clinical data sets and analyze the model.

The paper is organized as follows. The rest of this section introduces a mathematical model describing the in-host HIV infection dynamics. In section 2, a hierarchical NLME model is adopted, and parameters at both the individual and population levels are estimated. In section 3, analysis of the proposed model is performed and simulation studies are presented to demonstrate the analytical results. Finally, some discussions and remarks are made in section 4.

1.1. Mathematical model for in-host HIV dynamics. We develop a hierarchical mixed-effects model for HIV progression based on a simple in-host HIV infection dynamics model that involves variability among patients. The model we use to represent the dynamics of each individual is adopted from that proposed by Perelson et al. [1, 2, 9, 14]

$$\begin{cases} \frac{dS}{dt} &= \lambda - dS - (1-\eta)kVS \\ \frac{dI}{dt} &= (1-\eta)kVS - \delta I \\ \frac{dV}{dt} &= (1-\epsilon)N_T\delta I - cV \end{cases} \tag{1}$$

with given initial values for S, I, and V at time $t = t_0$.

This model includes the key dynamic compartments of uninfected target cells S, infected target cells I, and free virus V. The parameter λ denotes the rate at which uninfected target cells are created and d denotes the death rate of these cells. The infection rate k represents the rate of uninfected cells infected by the virus, and δ is the death rate of the infected target cells. Infected cells produce N_T free virus particles during a typical target cell life span, and the virus only leaves the compartment via natural death at rate c. The reader may refer to [1, 2, 9, 15] for a more detailed discussion of this model.

The drug efficacy parameter η models a reverse-transcriptase inhibitor (RTI) that blocks new infections, and ϵ represents the efficacy of protease inhibitor (PI). To specify the efficacy parameter η for the patients who are treated only using RTI, we employ the value of 80% reported and justified in the literature [9]. We assume that the values for both efficacy parameters η and ϵ to be 0.6 for each patient undergoing multidrug therapy, similar to the total drug efficacy of 80%. The definitions of the parameters are summarized in Table 1.

TABLE 1
Parameters in the in-host HIV infection model.

Parameter	Description	Units
λ	Birth rate of uninfected CD4+ T-cells	cells/[mm^3×day]
d	Death rate of uninfected CD4+ T-cells	1/day
k	Infection rate of CD4+ T-cells per virion	mm^3/[virions × day]
δ	Death rate of infected CD4+ T-cells	1/day
N_T	Burst size (number of virions released from an infected cell)	-
c	Natural death rate of virus	1/day
η	Efficacy of reverse transcriptase inhibitor	-
ϵ	Efficacy of protease inhibitor	-

1.2. HIV clinical data. The data employed to develop our model were collected by one of the authors (Choi) from patients at Severance Hospital. The ensemble provides partial observations that consist of measurements from the combined compartments of uninfected and infected of CD4+ T-cells and the censored RNA viral load measurements for 1030 patients. The measurement units of values are cells/μL for CD4 cells and copies/mL for viral load. The clinical data differs from patient to patient, both in duration and sampling frequency. The data set also contains prescription information of drug combination in antiretroviral treatment for all patients. The treated patients are considered to be successful if a viral load is maintained below 50 copies/mL. For some patients, viral suppression was not achieved with antiretroviral therapy, probably owing to poor patient adherence to drugs. Considering the feasibility, we estimated parameters from data of 176 patients: 89 patients undergoing multidrug therapy consisting of one or more RTIs and a protease inhibitor, and 87 patients who were treated using only RTIs.

2. Hierarchical mixed-effects model. There is a great deal of variability among patients, and dynamics may differ due to the differing crucial parameters. A hierarchical NLME model appears to be reasonable to explain the HIV dynamics at both the individual and population levels. A mixed-effects model represents two levels of variability, random variation among measurements within a given individual (intraindividual variation) and random variation among individuals (interindividual variation). One approach is to develop a model involving the distribution of the individual-specific parameters across the population of patients. In particular, the parameters in the in-host HIV infection model (1) are formulated as random variables to account for various sources of variability contained in the clinical data.

2.1. Parameter estimation of each individual. Intraindividual and interindividual variations are accommodated within the framework of a two-stage model. In this section, we formulate the estimation problem in the context of an in-host HIV dynamics model (1) to characterize the intraindividual variation. The data set includes longitudinal measurements for a population of patients with a different number of observations and sampling frequency. As mentioned above, a typical measurement includes the sum of uninfected and infected CD4+ T-cell counts ($S + I$) and the viral load (V).

It is known that the half-life of uninfected CD4+ T-cells is longer than that of infected CD4+ T-cells [12]. That is, the death rate of infected target cells is higher than the death rate of uninfected cells. Thus, we can convert the system (1) to a more convenient form (2) to estimate the parameters by introducing an auxiliary parameter $\mu \geq 0$ such that $\delta = d + \mu$:

$$\begin{cases} \frac{dS}{dt} &= \lambda - dS - (1-\eta)kVS \\ \frac{dI}{dt} &= (1-\eta)kVS - (d+\mu)I \\ \frac{dV}{dt} &= (1-\epsilon)N_T(d+\mu)I - cV. \end{cases} \tag{2}$$

Let $\tilde{\boldsymbol{\theta}}$ denote the individual-specific parameters in the model (2), and we will use the notation $\boldsymbol{\theta} = \ln(\tilde{\boldsymbol{\theta}})$ as parameters in the subsequent discussions. Given the j^{th} measurement $[S(t_j) + I(t_j), V(t_j)]^T$, $j = 1, \ldots, N$ for the individual, let $\boldsymbol{y}_j = [\log(S(t_j) + I(t_j)), \log(V(t_j))]^T$. We assume a statistical model for the observations of the form

$$\boldsymbol{Y}_j = \boldsymbol{f}(t_j; \boldsymbol{\theta}_0) + \boldsymbol{\varepsilon}_j, \qquad j = 1, \ldots, N,$$

where $\boldsymbol{Y}_j$ is a random vector composed of the log-scaled prediction $\boldsymbol{f}(t_j; \boldsymbol{\theta})$ at t_j with true parameter $\boldsymbol{\theta}_0$ and the measurement error $\boldsymbol{\varepsilon}_j \sim \mathcal{N}(\mathbf{0}, V_0)$. The log-scaled prediction is generated by taking $[\log(S(t_j) + I(t_j)), \log(V(t_j))]^T$ after solving the system of ordinary differential equations (2) for $S(t)$, $I(t)$ and $V(t)$, given values of parameter $\boldsymbol{\theta}$ and initial $[S(0), I(0), V(0)]^T$. Under the assumption $V_0 = \mathrm{diag}(\sigma_{0,1}^2, \sigma_{0,2}^2)$, the estimator $\hat{\boldsymbol{\theta}}$ and the bias-adjusted approximation for covariance $\hat{V}$ can be obtained using the weighted goodness-of-fit approach [6, 22]:

$$\hat{\boldsymbol{\theta}} = \arg\min_{\boldsymbol{\theta} \in \Omega_\theta} \sum_{j=1}^{N} [\boldsymbol{y}_j - \boldsymbol{f}(t_j; \boldsymbol{\theta})]^T V_0^{-1} [\boldsymbol{y}_j - \boldsymbol{f}(t_j; \boldsymbol{\theta})],$$

$$\hat{V} = \mathbf{diag}\left(\frac{1}{N - \kappa_\theta} \left(\sum_{j=1}^{N} [\boldsymbol{y}_j - \boldsymbol{f}(t_j; \hat{\boldsymbol{\theta}})][\boldsymbol{y}_j - \boldsymbol{f}(t_j; \hat{\boldsymbol{\theta}})]^T \right)_{ii} \right),$$

where κ_θ is the number of parameters. As $\boldsymbol{\theta}_0$ and V_0 are both unknown and coupled in the system of equations, the process is implemented iteratively to avoid computational complexity [6]. The details are given in section 5.

We estimate the parameters of the in-host HIV progression model (2) for 176 HIV patients undergoing therapies based on partial state observations $S + I$ and V. The observed quantities display a high degree of interpatient variability, including initial status and disease progression. The fitted data for two typical cases can be viewed in Figure 1, where the solid lines represent the simulations corresponding to the optimized parameters. Patient A with initial CD4 cell counts of 500 cells/μL was treated and exhibited suppressed viral loads. The other patient B who was at the AIDS stage at the beginning has reduced and maintained low viral loads due to the treatment.

2.2. Model reduction. The parameters are formulated as random variables in the mixed effects model to account for variability at both the individual and population levels. This model study requires a procedure to estimate the distribution of parameters, which is a formidable challenge if the dimension of the parameters is high. We employ a model-reduction technique in which the model fits the data with a minimal set of parameters [4, 16]. In this approach, we first rank the parameters to determine which are the most crucial to the HIV infection dynamics. Then, we use a nested model comparison test to decide whether the data can be adequately described by the surrogate model.

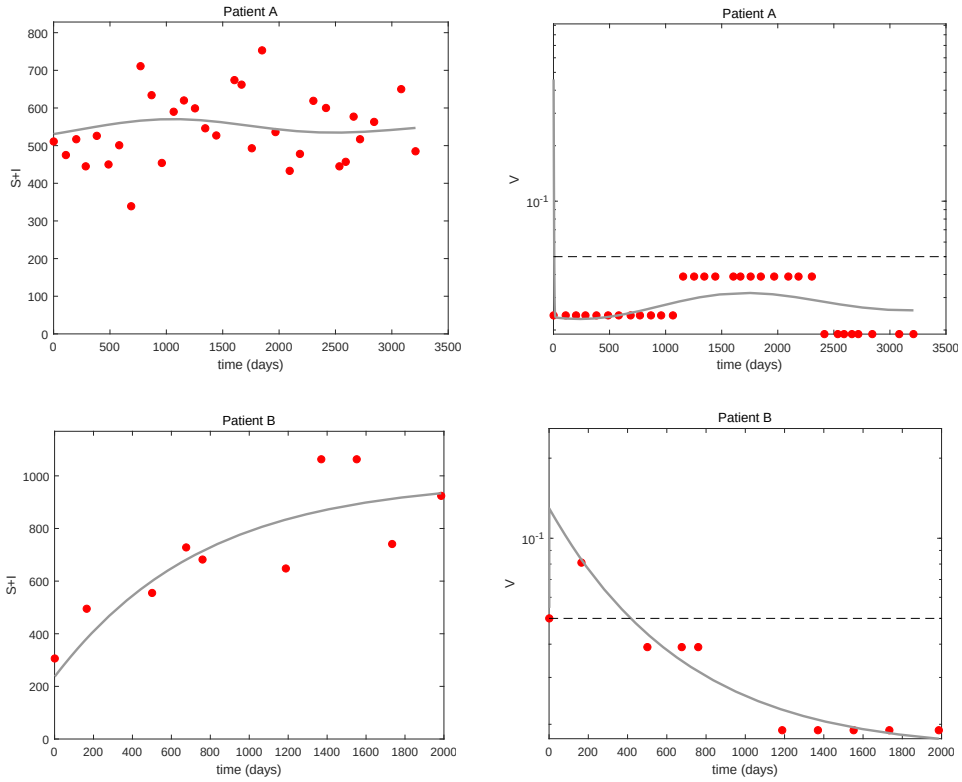

FIG. 1. *The model fit (solid line) to time series data (circles) for patient A (top) and patient B (bottom). Fit of model using estimated parameters to the CD4+ T-cell counts $S(t) + I(t)$ (left) and viral load $V(t)$ (right) are presented. The suppression level of viral loads (dashed line,* 0.05 *copies/μL) is also displayed for reference.*

2.2.1. Parameter ranking via sensitivity analysis. We investigate the sensitivity of the model with respect to parameters. The sensitivities defined by

$$[F(\boldsymbol{\theta})]_{j,k} = \frac{\partial \boldsymbol{f}(t_j;\boldsymbol{\theta})}{\partial \boldsymbol{\theta}_k}$$

can be computed by solving the sensitivity equations.

The order of parameters is given according to the sensitivity when the dependency on the previous parameters was removed. This can be implemented by using a QR decomposition of the sensitivity matrix $F(\boldsymbol{\theta})$, whose details are given in section 5. The results of the parameter ranking for two patients are presented in Figure 2.

2.2.2. Model comparison. Under the assumption that the measurement errors ε_j, $j = 1, 2, \ldots, N$ are normally distributed, Akaike information criterion (AIC) can be applied in the framework of the least-squares method [6, 4, 7]

$$\mathrm{AIC} = N\nu \ln\left(\frac{1}{N\nu}\sum_{j=1}^{N}\left[\boldsymbol{y}_j - \boldsymbol{f}(t_j;\hat{\boldsymbol{\theta}})\right]^T\left[\boldsymbol{y}_j - \boldsymbol{f}(t_j;\hat{\boldsymbol{\theta}})\right]\right) + 2(\kappa_\theta + 1),$$

where N is the number of measurements, ν is the dimension of measurements, and κ_θ is the number of parameters. This criterion balances the goodness of fit and the

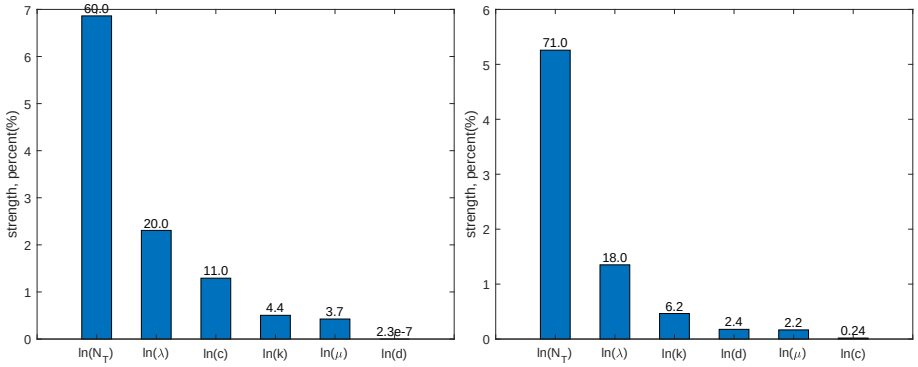

FIG. 2. *Parameter ranking based on the orthogonalization of the sensitivity matrix for patient A (left) and patient B (right).*

complexity of model by incorporating the squared sum of errors and the dimension of the parameters. Because AIC may perform poorly if the sample size is small relative to the total number of estimated parameters, we use a variation suggested for small samples [3, 6]:

$$\mathrm{AIC}_c = \mathrm{AIC} + \frac{2\kappa_\theta(\nu + \kappa_\theta + 1)}{N - (\nu + \kappa_\theta + 1)}.$$

To accomplish the goal to fit the data with a minimal set of parameters, we generate nested models based on the parameter ranking for each patient. First, we estimate only the most important parameter and fix the other parameters as the median of individually estimates whose distributions are mostly asymmetric. Then, we estimate the two most important parameters and repeat the process by increasing the number of parameters to be estimated according to the ranking. Nested models are compared using a small-sample AIC to determine the best approximating model, which is the one with the minimum AIC. The results of the model comparison for two patients are presented in Table 2. For the case of patient A, the parameters were ranked in order of decreasing sensitivity, given as $N_T, \lambda, c, k, \delta$. We determine that the minimal set of parameters is $\{N_T, \lambda, c, k\}$ with the minimum AIC value -199.7730. Similarly, we conclude that one parameter $\{N_T\}$ can adequately describe the data for patient B.

TABLE 2
Model comparison results for patient A (left) and patient B (right).

$\boldsymbol{\theta}$	AIC
N_T	-113.1571
N_T, λ	-110.9056
N_T, λ, c	-108.7563
N_T, λ, c, k	-199.7730
N_T, λ, c, k, δ	-199.0503

$\boldsymbol{\theta}$	AIC
N_T	-100.6845
N_T, λ	-96.2909
N_T, λ, k	-89.5633
N_T, λ, k, d	-80.5865
N_T, λ, k, d, δ	-57.2201

Our goal is to reduce the number of random parameters which reflect the population level understanding of HIV dynamics. However, the best approximating model, or the minimal set of parameters that is sufficient to describe the data, differs from patient to patient. We present the frequency of the selected parameters as a result of model reduction in Table 3. The minimal set of parameters is $\{N_T\}$ for 58 patients

TABLE 3
Frequency of minimal set of parameters as a result of model reduction.

Minimal set of parameters	Counts	Minimal set of parameters	Counts
N_T	58	c,d,λ	2
c	44	N_T,d,λ,k	2
k	12	c,N_T,d,λ	2
N_T,d,k,λ	5	c,N_T	1
N_T,d,k	4	c,N_T,k	1
N_T,λ	3	d	1
c,λ,k	3	c,d,N_T	1
N_T,λ,d	3	c,N_T,d,k	1
N_T,d,λ	3	k,c,N_T,d	1
c,d,k	2	c,k,N_T,d	1
		⋮	⋮
c,λ,d	2	⋮	⋮

and $\{c\}$ for 44 patients, and we determined N_T and c to be formulated as random variables.

2.3. Estimation of population parameters. After establishing the individual-level model, we seek a population-level understanding of HIV progression. We estimate the distribution of random variables across the population of patients from the individual-specific parameter values using the global two-stage (GTS) method [10].

Let $\tilde{\boldsymbol{\theta}}_i$ denote the individual-specific parameters for patient i and use $\boldsymbol{\theta}_i = \ln(\tilde{\boldsymbol{\theta}}_i)$ as in the previous sections. Given the measurement $\tilde{\boldsymbol{y}}_i$ for the ith individual, let $\boldsymbol{y}_i = \log(\tilde{\boldsymbol{y}}_i)$ and let $\boldsymbol{f}_i(\boldsymbol{\theta}_i)$ denote the log-scaled model prediction, a collection of values for all time t_j with his or her parameter $\boldsymbol{\theta}_i$.

Incorporating the uncertainty of estimation in $\boldsymbol{\theta}_i$ based on the asymptotic theory, it is assumed that $\boldsymbol{\theta}_i \sim \mathcal{N}(\boldsymbol{\theta^*}, C_i + D)$, such that the two-stage model may be written as

Stage 1 (intra-individual variation)

$$\boldsymbol{y}_i = \boldsymbol{f}_i(\boldsymbol{\theta}_i) + \boldsymbol{\varepsilon}_i, \qquad \boldsymbol{\varepsilon}_i|\boldsymbol{\theta}_i \sim \mathcal{N}(\mathbf{0}, V_i)$$

Stage 2 (inter-individual variation)

$$\boldsymbol{\theta}_i = \boldsymbol{\theta^*} + \boldsymbol{b_i} + \boldsymbol{e}_i^*, \quad \boldsymbol{b_i} \sim \mathcal{N}(\mathbf{0}, D), \quad \boldsymbol{e}_i^* \sim \mathcal{N}(\mathbf{0}, C_i).$$

In implementing this algorithm, an estimate of the asymptotic covariance matrix C_i for individual i would be used, where

$$C_i = \left(\sum_{j=1}^{N} [K_j(\hat{\boldsymbol{\theta}}_{\boldsymbol{i}})]^T \hat{V}^{-1} [K_j(\hat{\boldsymbol{\theta}}_{\boldsymbol{i}})] \right)^{-1}, \quad K_j(\boldsymbol{\theta}_{\boldsymbol{i}}) = \frac{\partial \boldsymbol{f}(t_j; \boldsymbol{\theta}_{\boldsymbol{i}})}{\partial \boldsymbol{\theta}_{\boldsymbol{i}}},$$

and $\boldsymbol{\theta}$ and D can be estimated by minimizing the negative loglikelihood

$$\mathcal{L}_{\mathrm{GTS}}(\boldsymbol{\theta^*}, D) = \sum_{i=1}^{m} \ln |C_i + D| + \sum_{i=1}^{m} (\boldsymbol{\theta}_i - \boldsymbol{\theta^*})^T (C_i + D)^{-1} (\boldsymbol{\theta}_i - \boldsymbol{\theta^*}).$$

We apply the GTS method to estimate the distribution of parameters formulated as random variables, and their corresponding statistical inference results are presented in Table 4. The joint distribution and the marginal distributions are displayed for the estimated parameters $\ln(N_T)$ and $\ln(c)$ in Figure 3. We also present the joint and marginal distributions of N_T and c in Figure 4.

TABLE 4
Statistical results for the parameters $\ln(N_T)$ *and* $\ln(c)$ *estimated using GTS method.*

	Parameter	Estimate
Mean	$\ln(N_T)$	3.0439
	$\ln(c)$	1.4901
Covariance	$(\ln(N_T), \ln(N_T))$	4.6290
	$(\ln(c), \ln(c))$	7.0640
	$(\ln(N_T), \ln(c))$	4.3613

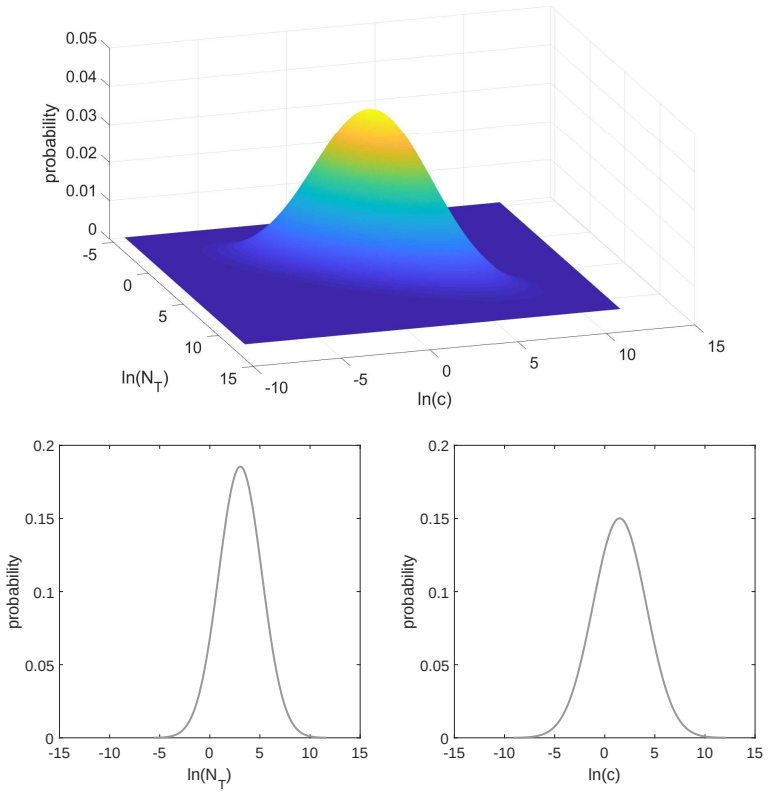

FIG. 3. *The joint distribution of* $\ln(N_T)$ *and* $\ln(c)$ *(top) and the corresponding marginal distributions of* $\ln(N_T)$ *and* $\ln(c)$ *(bottom) obtained by applying GTS method.*

3. Analysis of ordinary differential equations with random coefficients. In this section, we carry out an analysis of the model (3) established incorporating both individual- and population-level variations via the introduction of random parameters. Let $(\Omega, \mathcal{F}, P)$ denote a complete probability space. Ω is the set of all possible outcomes, $\mathcal{F} \subset 2^{\Omega}$ is the σ-algebra of events, and $P : \mathcal{F} \to [0, 1]$ is a probability measure. We formulate random variables $N_T(\omega)$ and $c(\omega)$, where $\omega \in \Omega$.

$$\begin{cases} \frac{dS}{dt} &= \lambda - dS - kVS \\ \frac{dI}{dt} &= kVS - \delta I \\ \frac{dV}{dt} &= N_T(\omega)\delta I - c(\omega)V \end{cases} \tag{3}$$

with given initial values for S, I, and V at time $t = t_0$.

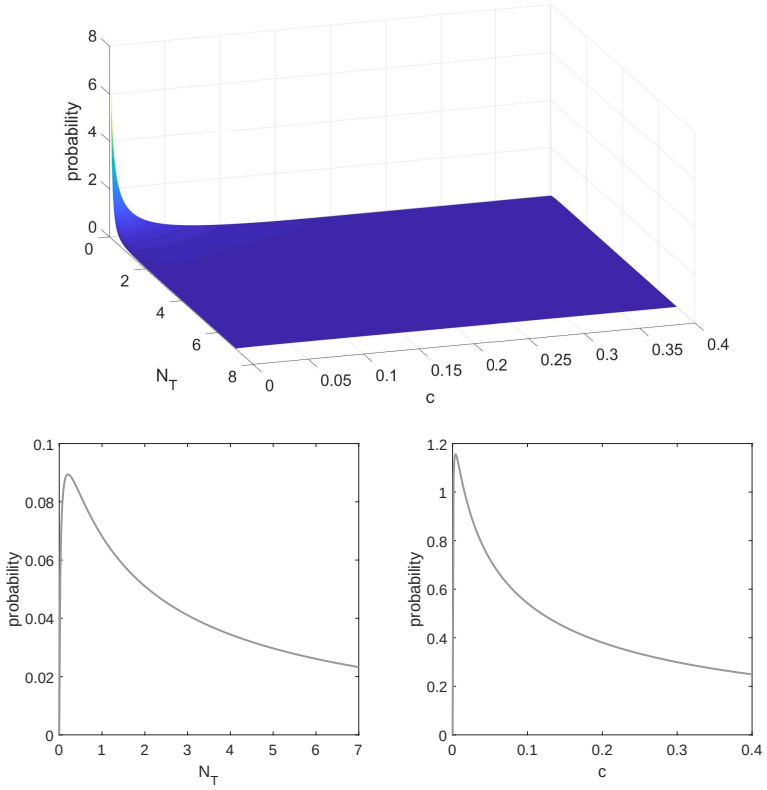

FIG. 4. *The joint distribution of N_T and c (top) and the corresponding marginal distributions of N_T and c (bottom) obtained by applying GTS method.*

To ensure the nonnegativity of solutions and to analyze asymptotic behavior, we assume that there are $c_{\min}, c_{\max}, N_{T\max} \in (0, \infty)$ such that

$$c_{\min} \le c(\omega) \le c_{\max} \quad \text{and} \quad N_T(\omega) \le N_{T\max}. \tag{4}$$

For the condition (4) for $N_T(\omega)$ and $c(\omega)$, as a practical example, N_T and c could have a truncated log-normal distribution.

3.1. Existence and uniqueness. The existence and uniqueness of a solution to (3) can be obtained by applying the following theorem (see [18]).

THEOREM 3.1. *Consider the stochastic differential equation*

$$d\boldsymbol{x}(t) = \boldsymbol{g}(t, \boldsymbol{x})dt + \boldsymbol{\sigma}(t, \boldsymbol{x})dB_t, \qquad t \in [0, T], \tag{5}$$

where $\boldsymbol{x}(0) = \boldsymbol{z}$ is a random initial condition satisfying $\mathbf{E}\left[|\boldsymbol{z}|^2\right] < \infty$. Assume that

$$|\boldsymbol{g}(t, \boldsymbol{x})| + |\boldsymbol{\sigma}(t, \boldsymbol{x})| \le C(1 + |\boldsymbol{x}|) \qquad \forall \boldsymbol{x} \in \mathbf{R}^n, \tag{6}$$

and

$$|\boldsymbol{g}(t, \boldsymbol{x}) - \boldsymbol{g}(t, \boldsymbol{y})| + |\boldsymbol{\sigma}(t, \boldsymbol{x}) - \boldsymbol{\sigma}(t, \boldsymbol{y})| \le D|\boldsymbol{x} - \boldsymbol{y}| \qquad \forall \boldsymbol{x}, \boldsymbol{y} \in \mathbf{R}^n, \tag{7}$$

where C and D are constants. Then, (5) *has a unique t-continuous solution $\boldsymbol{x}(t,\omega)$ satisfying*

$$\mathbf{E}\left[\int_0^T |\boldsymbol{x}(t)|^2 dt\right] < \infty.$$

We now state and prove an existence and uniqueness theorem for a solution to the system of ordinary differential equations (ODEs) with random coefficients.

THEOREM 3.2. *For any positive initial value, there is a unique solution to the system of random ODEs* (3).

Proof. Let $\tilde{\boldsymbol{x}} = [S, I, V]$, and define $\tilde{\boldsymbol{g}} : \mathbf{R}_+ \times \mathbf{R}^3 \to \mathbf{R}^3$ by

$$\tilde{\boldsymbol{g}}(t, \tilde{\boldsymbol{x}}) = \begin{bmatrix} \lambda - dS - kVS \\ kVS - \delta I \\ N_T \delta I - cV \end{bmatrix}.$$

Then, (3) can be rewritten by

$$\begin{cases} \frac{d\tilde{\boldsymbol{x}}}{dt} = \tilde{\boldsymbol{g}}(t, \tilde{\boldsymbol{x}}), \\ \tilde{\boldsymbol{x}}(0) = \tilde{\boldsymbol{x}}_0, \end{cases}$$

and $\boldsymbol{\sigma}(t, \tilde{\boldsymbol{x}}) = \mathbf{0}$.

In order to use Theorem 3.1, let $\boldsymbol{x} = [\tilde{\boldsymbol{x}}, \boldsymbol{z}(\omega)]^T$ with a random variable $\boldsymbol{z}(\omega) = [N_T(\omega), c(\omega)]^T$ satisfying $\mathbf{E}\left[|\boldsymbol{z}|^2\right] < \infty$, and let $\boldsymbol{g} = [\tilde{\boldsymbol{g}}, 0]^T$. Then, consider the augmented system

$$\begin{cases} \frac{d\boldsymbol{x}}{dt} = \boldsymbol{g}(t, \boldsymbol{x}), \\ \boldsymbol{x}(0) = \boldsymbol{x}_0. \end{cases}$$

Note that $|\tilde{\boldsymbol{g}}(t, \boldsymbol{x})| = |\boldsymbol{g}(t, \boldsymbol{x})|$.

To verify the condition (7), we show that $\tilde{\boldsymbol{g}}$ is locally Lipschitz continuous. Because the derivative of $\tilde{\boldsymbol{g}}$

$$\nabla \tilde{\boldsymbol{g}} = \begin{bmatrix} -d - kV & 0 & -kS \\ kV & -\delta & kS \\ 0 & N_T(\omega)\delta & -c(\omega) \end{bmatrix}$$

is continuous and locally bounded; $\tilde{\boldsymbol{g}}$ is locally Lipschitz continuous.

Now, we have

$$|\tilde{\boldsymbol{g}}(t, \boldsymbol{x})| = \left| \begin{bmatrix} \lambda - dS - kVS \\ kVS - \delta I \\ N_T \delta I - cV \end{bmatrix} \right| \leq \left| \begin{bmatrix} \lambda \\ 0 \\ 0 \end{bmatrix} \right| + \left| \begin{bmatrix} -dS - kVS \\ kVS - \delta I \\ N_T \delta I - cV \end{bmatrix} \right| = \lambda + \left| \begin{bmatrix} -dS - kVS \\ kVS - \delta I \\ N_T \delta I - cV \end{bmatrix} \right|.$$

Because $\tilde{\boldsymbol{g}}$ is locally Lipschitz continuous, there is a constant $\hat{D}$ such that

$$\left| \begin{bmatrix} -dS - kVS \\ kVS - \delta I \\ N_T \delta I - cV \end{bmatrix} \right| = |\tilde{\boldsymbol{g}}(t, \boldsymbol{x}) - \tilde{\boldsymbol{g}}(t, \mathbf{0})| \leq \hat{D}|\boldsymbol{x}|,$$

and hence,

$$|\tilde{\boldsymbol{g}}(t, \boldsymbol{x})| \leq \lambda + \hat{D}|\boldsymbol{x}| \leq C(1 + |\boldsymbol{x}|),$$

where $C = \max(\lambda, \hat{D})$.

By Theorem 3.1, there is a unique solution to the random ODE system (3). ∎

3.2. Nonnegativity. We show that the model proposed in this paper possesses nonnegative solutions, as this is essential for the model to be biologically feasible. We prove this positively invariant property in the following theorem.

THEOREM 3.3. *For any positive initial value, the solution* $\boldsymbol{x}(t)$ *to a random ODE system* (3) *will be positive.*

Proof. By Theorem 3.2, there is a unique local solution $\boldsymbol{x}(t)$ on $[0, \tau_e)$ for any positive initial value $\boldsymbol{x}_0$, where τ_e is the explosion time defined by (see [17])

$$\lim_{t \uparrow \tau_e} |\boldsymbol{x}(t)| = \infty.$$

To prove that the solution is global, we need to show that $\tau_e = \infty$. Let us define the stopping time τ_s:

$$\tau_s = \inf \{t \in [0, \tau_e) : S(t) \leq 0 \text{ or } I(t) \leq 0 \text{ or } V(t) \leq 0\}.$$

It is enough to show that $\tau_s = \infty$ to conclude the solution $\boldsymbol{x}(t) \in \mathbf{R}^3_+$ almost surely for $t \geq 0$.

We assume that $\tau_s < \infty$, which will lead to a contradiction. Define a function $\phi(\boldsymbol{x}(t)) : \mathbf{R}^3_+ \to \mathbf{R}^3_+$ by $\phi(\boldsymbol{x}(t)) = \ln(SIV)$. Then,

$$d\phi(\boldsymbol{x}(t)) = \left[\frac{\lambda}{S} - d - kV + k\frac{VS}{I} - \delta + N_T(\omega)\delta\frac{I}{V} - c(\omega)\right] dt.$$

From (4), we obtain

$$d\phi(\boldsymbol{x}(t)) \geq [-d - kV - \delta - c_{\max}]\, dt.$$

Therefore,

$$\phi(\boldsymbol{x}(t)) \geq \phi(\boldsymbol{x}_0) - \int_0^t kV(s)ds - (d + \delta + c_{\max})t.$$

Note that the right-hand side is finite for $t < \tau_s < \tau_e$. Letting $t \to \tau_s$ leads to the contradiction

$$-\infty = \lim_{t \to \tau_s} \phi(\boldsymbol{x}(t)) \geq \phi(\boldsymbol{x}_0) - \lim_{t \to \tau_s} \int_0^t kV(s)ds - \lim_{t \to \tau_s} (d + \delta + c_{\max})t > -\infty.$$

Consequently, $\tau_s = \infty$ almost certainly. ∎

3.3. Asymptotic behavior. In this section, we investigate the asymptotic behavior of solutions, which is of great interest in the study of biological systems. We carry out analysis on the stochastic equilibrium, and the results are illustrated by numerical simulations. First, we establish the conditions for extinction in the following theorem.

THEOREM 3.4. *Consider the random ODE system* (3) *with the initial condition in* $\mathbf{R}^3_+$. *Assume that* N_T *and* c *follow a multivariate truncated log-normal distribution. If* $c_{min} d - k\lambda N_{T\,max} > 0$, *then* $I(t)$ *and* $V(t)$ *tend to zero exponentially with probability one.*

Proof. The first equation of our random ODE system (3),

$$\frac{dS}{dt} = \lambda - dS - kVS \leq \lambda - dS,$$

yields

$$0 \le S(t) \le \frac{\lambda}{d} - \left(\frac{\lambda}{d} - S_0\right) e^{-dt},$$

which further implies bounds on the state S,

$$\begin{cases} S(t) \le \frac{\lambda}{d} & \text{if } S_0 \le \frac{\lambda}{d}, \\ S(t) \le S_0, & \text{otherwise.} \end{cases}$$

If we assume that $S_0 \le \frac{\lambda}{d}$, then

$$\begin{bmatrix} \frac{dI}{dt}(t) \\ \frac{dV}{dt}(t) \end{bmatrix} = \begin{bmatrix} -\delta & kS(t) \\ N_T(\omega)\delta & -c(\omega) \end{bmatrix} \begin{bmatrix} I(t) \\ V(t) \end{bmatrix} \le \begin{bmatrix} -\delta & k \cdot \frac{\lambda}{d} \\ N_T(\omega)\delta & -c(\omega) \end{bmatrix} \begin{bmatrix} I(t) \\ V(t) \end{bmatrix}.$$

We define $\boldsymbol{x} = \left[\begin{smallmatrix} I \\ V \end{smallmatrix}\right]$ and $A = \left[\begin{smallmatrix} -\delta & k \cdot \frac{\lambda}{d} \\ N_T(\omega)\delta & -c(\omega) \end{smallmatrix}\right]$ to formulate a system $\frac{d\boldsymbol{x}}{dt} = A\boldsymbol{x}$ whose solutions tend to zero exponentially with probability one.

By solving the characteristic equation

$$\nu^2 + (\delta + c(\omega))\nu + c(\omega)\delta - k\frac{\lambda}{d}N_T(\omega)\delta = 0,$$

we obtain eigenvalues

$$\nu_1 = \frac{1}{2}\left\{-(\delta + c(\omega)) + \sqrt{(\delta + c(\omega))^2 - 4\left(c(\omega)\delta - k\frac{\lambda}{d}N_T(\omega)\delta\right)}\right\},$$

$$\nu_2 = \frac{1}{2}\left\{-(\delta + c(\omega)) - \sqrt{(\delta + c(\omega))^2 - 4\left(c(\omega)\delta - k\frac{\lambda}{d}N_T(\omega)\delta\right)}\right\}.$$

Both eigenvalues are real, and $\nu_2 < 0$ because

$$(\delta + c(\omega))^2 - 4\left(c(\omega)\delta - k\frac{\lambda}{d}N_T(\omega)\delta\right) = (\delta - c(\omega))^2 + 4k\frac{\lambda}{d}N_T(\omega)\delta > 0.$$

In order for ν_1 to be negative, it is required that

$$c(\omega)\delta - k\frac{\lambda}{d}N_T(\omega)\delta > 0.$$

It then follows from the assumption (4) that

$$c(\omega)\delta - k \cdot \frac{\lambda}{d} \cdot N_T(\omega)\delta > c_{\min}\delta - k \cdot \frac{\lambda}{d} \cdot N_{T\max}\delta = c_{\min}\delta\left(1 - \frac{k\lambda N_{T\max}}{c_{\min}d}\right).$$

Hence, we show that $I(t)$ and $V(t)$ tend to zero under the condition $c_{\min}d - k\lambda N_{T\max} > 0$ for case $S_0 \le \frac{\lambda}{d}$. Using similar arguments, one can obtain the same condition for extinction in the case of $S_0 > \frac{\lambda}{d}$. Therefore, we conclude that solutions extinct if $c_{\min}d - k\lambda N_{T\max} > 0$. ∎

According to our analytical results, both the infected cells and the virus particles exponentially tend to zero with probability one under the conditions specified in Theorem 3.4. The numerical simulations in Figure 5 support these results, illustrating extinction of the infected cells and the virus. We assume that all the initial values

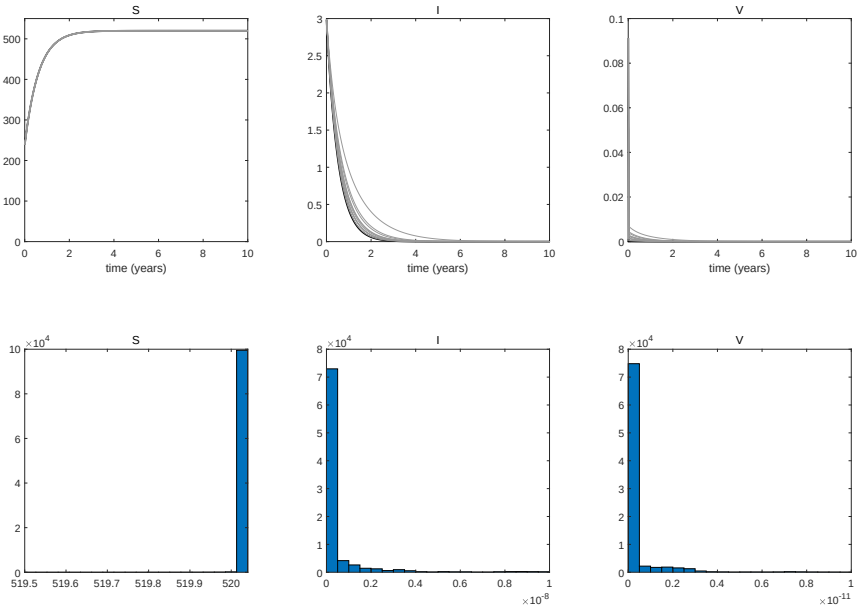

FIG. 5. *The trajectories (gray) of uninfected cells, infected cells, and the virus using samples of N_T and c under the condition for extinction are plotted (top). The dynamics of each state corresponding to the mean value of N_T and c are also displayed (black solid). Frequency histograms of S, I, and V based on $100,000$ simulations at time $t = 20$ using sample pairs of N_T and c are shown (bottom).*

and system parameters, other than N_T and c, are fixed as the median of individually estimated values; in other words, we have $S(0) = 238.4283, I(0) = 2.9865, V(0) = 0.0913, \lambda = 2.3039, d = 0.0044, k = 0.0025,$ and $\mu = 0.001$. The values of N_T and c are sampled following the truncated log-normal distribution, where $N_{T\max}$ and $c_{\min}$ are chosen to satisfy the condition $c_{\min}d - k\lambda N_{T\max} > 0$. The trajectories of each state are plotted, demonstrating that both I and V tend to zero asymptotically. Figure 5 also shows histograms of the approximate stationary distribution of the uninfected cells, infected cells, and the virus.

We now consider a more realistic example with parameters estimated from actual data in the previous section. That is, we keep all the parameters the same as in Figure 5, except for those formulated as random variables to account for variability. The joint distribution of N_T and c follows the truncated distribution of multivariate log-normal estimated using the global two-stage method. This choice of parameters does not satisfy the condition for extinction in Theorem 3.4. Figure 6 displays both trajectories and histograms of uninfected and infected CD4+ T-cells and viral load, illustrating persistence. The numerical results strongly indicate that the HIV infection model (3) has a stationary distribution, while we have not so far been able to prove this.

4. Discussions. We have presented a hierarchical mixed-effects model to account for HIV dynamics at both the individual and population levels. A simple in-host HIV model was adopted to represent the infection dynamics of each individual. The crucial parameters in the model were formulated as random variables to incorporate variability among patients, which was clear in the clinical data. Individual

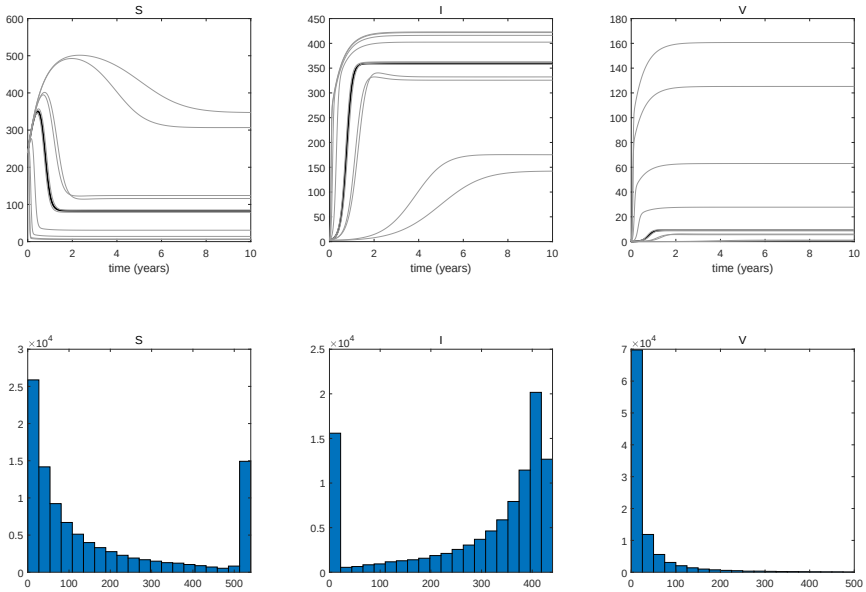

FIG. 6. *The trajectories (gray) of uninfected cells, infected cells, and the virus using samples of N_T and c following the truncated multivariate log-normal estimated by the global two-stage method are plotted (top). The dynamics of each state corresponding to the mean value of N_T and c are also displayed (black solid). Frequency histograms of S, I, and V based on* $100,000$ *simulations at time* $t = 20$ *using sample pairs of N_T and c are shown (bottom).*

parameter values and the distribution of random variables were estimated using the field data of 176 patients. We have also analyzed the proposed model with random inputs, showing the existence, uniqueness, and nonnegativity of the solutions. Then, we investigated asymptotic behaviors and established conditions for the extinction of a disease. Finally, numerical simulations exhibit the stationary distribution of both extinction and persistence cases.

The eventual goal of our research is to predict the future patterns of the response at each individual, taking uncertainty and population level variability into consideration. It will allow one to design different individual therapy regimes and to suggest best performance treatment strategies. This paper is only a first step in developing mixed effects models, which can be used to achieve eventual aims of prediction and control. One may study a more realistic version by improving several ways such as employing advanced parameter estimation techniques and researching on the efficacy of drug cocktails. We have left these for further investigations.

5. Appendix.

5.1. Parameter and covariance estimation. Let $\hat{\boldsymbol{\theta}}$ denote the estimated parameter obtained by solving the problem

$$\hat{\boldsymbol{\theta}} = \arg \min_{\boldsymbol{\theta} \in \Omega_\theta} \sum_{j=1}^{N} [\boldsymbol{y}_j - \boldsymbol{f}(t_j; \boldsymbol{\theta})]^T \hat{V}^{-1} [\boldsymbol{y}_j - \boldsymbol{f}(t_j; \boldsymbol{\theta})], \tag{8}$$

where V_0 is the covariance matrix of measurement error $\boldsymbol{\varepsilon}_j$, which is unknown in general.

It can be approximated by $\hat{V}$ in the following formula:

$$V_0 \approx \hat{V} = \mathbf{diag}\left(\frac{1}{N-\kappa_\theta}\left(\sum_{j=1}^{N}[\boldsymbol{y}_j - \boldsymbol{f}(t_j;\hat{\boldsymbol{\theta}})][\boldsymbol{y}_j - \boldsymbol{f}(t_j;\hat{\boldsymbol{\theta}})]^T\right)_{ii}\right), \tag{9}$$

where N is the number of measurement, κ_θ is the number of parameters, and $\hat{\boldsymbol{\theta}}$ is a parameter estimator. However, $\hat{V}$ and $\hat{\boldsymbol{\theta}}$ are coupled in the sense that computing $\hat{V}$ in (9) involves $\hat{\boldsymbol{\theta}}$ and estimating $\hat{\boldsymbol{\theta}}$ in (8) requires V_0.

We follow a standard practice of decoupling at a cost of iteration to take care of this coupled problem, which can be implemented as

1. Choose an initial guess for $\hat{V}$ as $\hat{V}^{(0)} = \boldsymbol{I}$ and estimate $\hat{\boldsymbol{\theta}}^{(0)}$ by the formula (8) and set $l = 0$.
2. Evaluate $\hat{V}^{(l+1)}$ with $\hat{\boldsymbol{\theta}}^{(l)}$ using (9).
3. Update $\hat{\boldsymbol{\theta}}$ from (8) with $\hat{V} = \hat{V}^{(l+1)}$ to obtain $\hat{\boldsymbol{\theta}}^{(l+1)}$.
4. Set $l = l + 1$ and return to step 2 until two successive estimates of iteration for $\hat{\boldsymbol{\theta}}$ are close enough.

As a result of this iterative process, we obtain both estimates $\hat{\theta}$ and $\hat{V}$.

5.2. Solving sensitivity equation. Let $\boldsymbol{f}(t_j;\boldsymbol{\theta}) = [f_1(t_j;\boldsymbol{\theta}), f_2(t_j;\boldsymbol{\theta})]^T = [\log(S(t_j)+I(t_j)), \log(V(t_j))]^T$ be the log-scaled prediction and define the sensitivity matrix as follows:

$$F(\boldsymbol{\theta}) = \begin{bmatrix} \frac{\partial f_1(t_1;\boldsymbol{\theta})}{\partial \lambda} & \frac{\partial f_1(t_1;\boldsymbol{\theta})}{\partial d} & \cdots & \frac{\partial f_1(t_1;\boldsymbol{\theta})}{\partial N_T} \\ \frac{\partial f_1(t_2;\boldsymbol{\theta})}{\partial \lambda} & \frac{\partial f_1(t_2;\boldsymbol{\theta})}{\partial d} & \cdots & \frac{\partial f_1(t_2;\boldsymbol{\theta})}{\partial N_T} \\ \vdots & \vdots & \ddots & \vdots \\ \frac{\partial f_1(t_N;\boldsymbol{\theta})}{\partial \lambda} & \frac{\partial f_1(t_N;\boldsymbol{\theta})}{\partial d} & \cdots & \frac{\partial f_1(t_N;\boldsymbol{\theta})}{\partial N_T} \\ \frac{\partial f_2(t_1;\boldsymbol{\theta})}{\partial \lambda} & \frac{\partial f_2(t_1;\boldsymbol{\theta})}{\partial d} & \cdots & \frac{\partial f_2(t_1;\boldsymbol{\theta})}{\partial N_T} \\ \frac{\partial f_2(t_2;\boldsymbol{\theta})}{\partial \lambda} & \frac{\partial f_2(t_2;\boldsymbol{\theta})}{\partial d} & \cdots & \frac{\partial f_2(t_2;\boldsymbol{\theta})}{\partial N_T} \\ \vdots & \vdots & \ddots & \vdots \\ \frac{\partial f_2(t_N;\boldsymbol{\theta})}{\partial \lambda} & \frac{\partial f_2(t_N;\boldsymbol{\theta})}{\partial d} & \cdots & \frac{\partial f_2(t_N;\boldsymbol{\theta})}{\partial N_T} \end{bmatrix}.$$

It tells us how much the prediction changes as each parameter θ_k perturbs ($k = 1, 2, \ldots, \kappa_\theta$).

Among several ways to compute this sensitivity matrix $F(\boldsymbol{\theta})$ ([6, see Chapter 3]), we approximate it by using the forward difference, e.g., the first element of $F(\boldsymbol{\theta})$ can be obtained by

$$\frac{\partial f_1(t_1;\boldsymbol{\theta})}{\partial \lambda} \approx \frac{f(t_j;\boldsymbol{\theta}+\boldsymbol{h}_1) - f(t_j;\boldsymbol{\theta})}{\|\boldsymbol{h}_1\|},$$

where $\|\cdot\|$ is the Euclidean norm in κ_θ-dimensional real vector space $\boldsymbol{R}^{\kappa_\theta}$ and $\boldsymbol{h}_1$ is a $\kappa_\theta \times 1$ vector whose entries are 0, except that the first one is chosen as a very small value. Here, each parameter is perturbed by 1% of it estimated value (i.e., $\boldsymbol{h}_1 = [0.01 * \lambda, 0, \ldots, 0]^T$).

Based on this sensitivity matrix $F(\boldsymbol{\theta})$, parameters are ranked by the following process. Note that the kth column of $F(\boldsymbol{\theta})$ is a sensitivity vector for the parameter θ_k, all parameters are in log-scale, and L2-norm is used to measure a vector. We compare the norm of sensitivity vectors corresponding to each parameter and rank

the one with the largest norm as the 1st because the larger norm represents the bigger impact on the dynamics. In Figure 2, $\ln(N_T)$ rank the 1st for both Patient A and Patient B. Then, we orthogonalize the remaining sensitivity vectors by removing the 1st-ranked direction and compare the norm of the resulting vectors to determine the 2nd one attaining the largest norm. The 2nd ranked parameter is $\ln(\lambda)$ for Patient A and Patient B, in Figure 2. The direction of 2nd-ranked sensitivity vector is removed from the remaining vectors, select the 3rd parameter and repeat this process until all the parameters are ranked.

REFERENCES

[1] B. M. Adams, H. T. Banks, M. Davidian, H.-D. Kwon, H. T. Tran, S. N. Wynne, and E. S. Rosenberg, *HIV dynamics: Modeling, data analysis, and optimal treatment protocols*, J. Comput. Appl. Math., 184 (2005), pp. 10–49.

[2] B. M. Adams, H. T. Banks, H.-D. Kwon, and H. T. Tran, *Dynamic multidrug therapies for HIV: Optimal and STI control approaches*, Math. Biosci. Eng., 1 (2004), pp. 223–241.

[3] K. Adoteye, H. T. Banks, K. Cross, S. Eytcheson, K. B. Flores, G. A. LeBlanc, T. Nguyen, C. Ross, E. Smith, M. Stemkovski, et al., *Statistical validation of structured population models for Daphnia magna*, Math. Biosci., 266 (2015), pp. 73–84.

[4] H. T. Banks, *Analysis of a quasi-chemical kinetic food chemistry model*, tech. report, North Carolina State University, Center for Research in Scientific Computation, 2016.

[5] H. T. Banks, S. Grove, S. Hu, and Y. Ma, *A hierarchical bayesian approach for parameter estimation in HIV models*, Inverse Problems, 21 (2005), p. 1803.

[6] H. T. Banks, S. Hu, and W. C. Thompson, *Modeling and inverse problems in the presence of uncertainty*, Monographs and Research Notes in Mathematics, Taylor and Francis, Hoboken, NJ, 2014, http://cds.cern.ch/record/1701411.

[7] H. T. Banks and M. L. Joyner, *AIC under the framework of least squares estimation*, Appl. Math. Lett., 74 (2017), pp. 33 – 45, https://doi.org/10.1016/j.aml.2017.05.005.

[8] S. Bonhoeffer, M. Rembiszewski, G. M. Ortiz, and D. F. Nixon, *Risks and benefits of structured antiretroviral drug therapy interruptions in HIV-1 infection*, AIDS, 14 (2000), pp. 2313–2322.

[9] D. S. Callaway and A. S. Perelson, *HIV-1 infection and low steady state viral loads*, Bull. Math. Biol., 64 (2002), pp. 29–64.

[10] M. Davidian, *Nonlinear models for repeated measurement data*, Routledge, 2017.

[11] A. T. Haase, K. Henry, M. Zupancic, G. Sedgewick, R. A. Faust, H. Melroe, W. Cavert, K. Gebhard, K. Staskus, Z.-Q. Zhang, et al., *Quantitative image analysis of HIV-1 infection in lymphoid tissue*, Science, 274 (1996), pp. 985–989.

[12] M. Hellerstein, M. Hanley, D. Cesar, S. Siler, C. Papageorgopoulos, E. Wieder, D. Schmidt, R. Hoh, R. Neese, D. Macallan, et al., *Directly measured kinetics of circulating T lymphocytes in normal and HIV-1-infected humans*, Nature Medicine, 5 (1999), p. 83.

[13] A. Herz, S. Bonhoeffer, R. M. Anderson, R. M. May, and M. A. Nowak, *Viral dynamics in vivo: Limitations on estimates of intracellular delay and virus decay*, Proc. Natl. Acad. Sci. USA, 93 (1996), pp. 7247–7251.

[14] T. Jang, J. Kim, H.-D. Kwon, and J. Lee, *Hybrid on-off controls for an HIV model based on a linear control problem*, J. Korean Math. Soc., 52 (2015), pp. 469–487, https://doi.org/10.4134/JKMS.2015.52.3.469.

[15] E. Jones, P. Roemer, M. Raghupathi, and S. Pankavich, *Analysis and simulation of the three-component model of HIV dynamics*, preprint, https://arxiv.org/abs/1312.3671 arXiv:1312.3671, https://arxiv.org/abs/1312.3671, 2013.

[16] B. F. Lund, H. E. Berntsen, and B. A. Foss, *Methods for parameter ranking in nonlinear, mechanistic models*, IFAC Proceedings Volumes, 38 (2005), pp. 578 – 583, https://doi.org/10.3182/20050703-6-CZ-1902.00097.

[17] X. Mao, *Stochastic Differential Equations and Applications*, Elsevier, New York, 2007.

[18] B. Øksendal, *Stochastic differential equations*, in Stochastic differential equations, Springer, 2003, pp. 65–84.

[19] A. S. Perelson and P. W. Nelson, *Mathematical analysis of HIV-1 dynamics in vivo*, SIAM Rev., 41 (1999), pp. 3–44.

[20] H. Putter, S. H. Heisterkamp, J. M. A. Lange, and F. De Wolf, *A Bayesian approach to parameter estimation in HIV dynamical models*, Stat. Med., 21 (2002), pp. 2199–2214.

[21] M. A. Stafford, L. Corey, Y. Cao, E. S. Daar, D. D. Ho, and A. S. Perelson, *Modeling plasma virus concentration during primary HIV infection*, J. Theoret. Biol., 203 (2000), pp. 285–301, https://doi.org/10.1006/jtbi.2000.1076.

[22] T. Vanni, J. Karnon, J. Madan, R. G. White, W. J. Edmunds, A. M. Foss, and R. Legood, *Calibrating models in economic evaluation*, Pharmacoeconomics, 29 (2011), pp. 35–49.

[23] H. Wu, *Statistical methods for HIV dynamic studies in AIDS clinical trials*, Stat. Methods Med. Res., 14 (2005), pp. 171–192.

[24] H. Wu and A. A. Ding, *Population HIV-1 dynamics in vivo: Applicable models and inferential tools for virological data from AIDS clinical trials*, Biometrics, 55, pp. 410–418, https://doi.org/10.1111/j.0006-341X.1999.00410.x.